Composites: Part A 207 (2026) 109851

Contents lists available at ScienceDirect

Composites Part A

journal homepage: www.elsevier.com/locate/compositesa

Bayesian optimization and guided over-instrumented gripper design for thermoforming of composite materials

Frank Doehner [a,b,1,*], Johannes Mitsch [c,1], Saksham Kiroriwal [b,1], Shahenda Youssef [a,b], Georg Zeeb [c,d], Frank Henning [c,d], Luise Kärger [c], Jürger Beyerer [a,b,**]

[a] Vision and Fusion Laboratory (IES), Karlsruhe Institute of Technology (KIT), Germany
[b] Fraunhofer Institute of Optronics, System Technologies and Image Exploitation (IOSB), Germany
[c] Lightweight Engineering, Institute of Vehicle System Technology (FAST), Karlsruhe Institute of Technology (KIT), Germany
[d] Fraunhofer Institute of Chemical Technology (ICT), Germany

ARTICLE INFO

Keywords:
Composite forming
Process optimization
Finite element method
Bayesian optimization
Gaussian process regression

ABSTRACT

This work investigates the application of Bayesian Optimization for optimizing process settings in the thermoforming of continuous fiber-reinforced thermoplastic composites. The optimization addresses a high-dimensional design problem involving the positions and forces of tension grippers, aiming to minimize wrinkle formation based on computationally expensive finite element simulations. Advanced Bayesian Optimization techniques, including Log Expected Improvement and Trust Region Bayesian Optimization, demonstrate superior performance compared to standard methods, achieving large wrinkle reduction with fewer simulation evaluations. A sensitivity analysis based on the learned Gaussian process surrogate model is performed, providing quantitative insights into the relative influence of individual gripper parameters. Building on the optimized baseline configuration, the Trust Region based Bayesian Optimization is utilized to identify promising regions for over-instrumentation beyond basic parameter tuning. The approach leverages the previously obtained solution in the 16-dimensional optimization domain together with a one-dimensional positional exploration of the added gripper to identify Trust Regions. The results show that strategic over-instrumentation combined with local re-optimization can yield significant improvements in forming quality with low additional effort, demonstrating the effectiveness of Bayesian Optimization for simulation-based optimization of immature manufacturing processes.

1. Introduction

1.1. Motivation

The utilization of thermoplastic tapes in the manufacturing of continuous fiber-reinforced thermoplastics (CoFRTPs) enables the large-scale production of structural components with optimal lightweight potential. The division of the production process into the steps of tape laying, consolidation to a laminate, and thermoforming has been demonstrated to result in highly productive component manufacturing [1]. Coupled with the recyclability and weldability of thermoplastic matrix systems, this has given rise to a growing interest in these semi-finished products in the continuously expanding aviation sector. However, this sector in particular has the highest requirements for robust and defect-free component production [2]. To meet these requirements, all process steps must be mastered, and the quality of the resulting components is determined by the quality of the sequentially executed process steps. Since thermoforming is the most complex and critical step in manufacturing CoFRTP components, it poses significant economic risks and process challenges for the entire value chain and the final component quality.

Extensive research has demonstrated the influence of key process parameters on the geometry and mechanical properties of formed parts such as temperature [3,4], gripper positioning [5–8], and initial fiber orientation [9,10]. However, experimental optimization of these parameters is often both time-consuming and costly. As a result, the Finite Element Method (FEM) has emerged as a key tool for virtually designing and optimizing manufacturing processes for continuous fiber-reinforced plastics (CoFRPs). Due to the high dimensionality of the resulting parameter space, advanced optimization strategies are required to efficiently explore the design space and identify optimal

* Corresponding author at: Vision and Fusion Laboratory (IES), Karlsruhe Institute of Technology (KIT), Germany.
** Corresponding author.
E-mail addresses: frank.doehner@kit.edu (F. Doehner), juergen.beyerer@iosb.fraunhofer.de (J. Beyerer).
[1] These authors contributed equally to this work.

https://doi.org/10.1016/j.compositesa.2026.109851
Received 25 February 2026; Received in revised form 2 April 2026; Accepted 14 April 2026
Available online 22 April 2026

process configurations with a limited number of simulations. BO is well suited for this purpose, as it is specifically designed to optimize computationally expensive black box functions such as those encountered in forming simulations for CoFRPs.

1.2. Related work

The following section reviews prior work relevant to simulation-driven optimization of composite forming. First, the physical mechanisms governing defect formation and the development of high-fidelity FEM forming simulations are summarized. Subsequently, existing approaches to simulation-driven optimization and surrogate learning are discussed, followed by Bayesian Optimization (BO) methods and their application to composite forming problems.

1.2.1. Forming physics and finite element simulation of composite forming

Finite element simulation plays a central role in understanding and improving the forming of continuous fiber-reinforced composites, including both dry textile systems and thermoplastic laminates. Recent reviews [11–15] summarize how forming feasibility and defect formation depend on geometry, layup, and process settings, and emphasize that credible virtual process design increasingly relies on high-fidelity simulation rather than trial-and-error approaches.

The physical mechanisms governing wrinkle formation and related defects motivate why optimization cannot rely on simple heuristics. Classic work by Tam and Gutowski [16,17] established how kinematic constraints and inter-ply slip influence the ability to form aligned fiber laminates into complex shapes, providing a mechanistic basis for forming feasibility. Building on these mechanics-based considerations, Gutowski et al. [18] derived scaling relationships linking laminate mechanics and compression states to the onset of wrinkling. Experimental investigations such as Hallander et al. [19] further demonstrated how wrinkles can originate from localized compression and instability mechanisms that are not evident from global loading conditions alone. Together, these studies highlight that defect formation results from strongly coupled and highly localized interactions between tension, shear, bending, and slip.

To capture these mechanisms in FEM-based forming simulations of CoFRPs, increasingly sophisticated material models have been developed. Examples include decoupled membrane–bending formulations [20,21], viscoelastic constitutive models for rate-dependent deformation [22,23], and temperature-dependent material descriptions including crystallization effects [24–26]. Additional developments address inter-ply slip mechanics [27–29] and thickness evolution during forming [30,31]. While these advances significantly improve predictive capability, they also increase computational cost, making individual forming simulations expensive and motivating sample efficient optimization strategies under limited simulation budgets.

1.2.2. Simulation-driven optimization and surrogate learning from forming simulations

Simulation-driven optimization of composite forming processes has been studied for several decades and predates modern machine learning. Early work includes FEM-based optimal-design formulations for composite thermoforming by Hsiao and Kikuchi [32] and process optimization studies for multilayer woven fabric forming such as Vanclooster et al. [3]. More recently, optimization has been embedded into broader engineering workflows, for example in the forming optimization within a CAE-chain described by Kärger et al. [33]. These contributions support the view that FEM simulation can act as the primary experimental surrogate in a design loop, but they also highlight that computational cost becomes the limiting factor as the parameter space grows. To reduce the number of expensive simulations, surrogate and learning-based approaches explicitly treat FEM simulation as a generator of training data. Pfrommer et al. [34] demonstrated deep neural networks trained on finite-element draping outputs to predict full-field quantities such as shear-angle distributions and thereby accelerate optimization. Zimmerling et al. [35] proposed machine-learning-assisted formability assessment to speed iterative improvement, and later advanced reinforcement learning to estimate process parameters across variable component geometries [36]. Tan and Nhat [37] provides an additional example of machine-learning-based prediction and optimization of thermoforming process parameters from simulation-informed data.

Recent work aims at learned surrogate simulators that approximate the full forming response, thereby reducing the need for repeated high-fidelity FEM evaluations. For thermoforming of CoFRTPs, Würth et al. [38] propose algebraic-hierarchical graph neural network simulators trained on high-fidelity Abaqus/Explicit simulations based on experimentally validated forming models. The approach builds on the learned-simulation framework ROBIN introduced by Würth et al. [39] for physics-informed surrogate simulation of nonlinear solid mechanics. The resulting simulator predicts global draw-in and local wrinkling for unseen process settings while reducing runtimes from minutes to seconds, enabling near real-time evaluation in iterative workflows and providing a promising route to accelerate simulation-driven optimization of forming processes.

1.2.3. Bayesian optimization for expensive simulations and applications to composite forming

BO provides a principled framework for sample-efficient optimization of expensive black-box objectives, which matches the role of high-fidelity forming simulations. The computer-experiments perspective introduced by Sacks et al. [40] motivates Gaussian Process (GP) surrogate modeling for deterministic simulators, and the Expected Improvement (EI) based Efficient Global Optimization framework was formalized by Jones et al. [41]. Broader surrogate-based optimization guidance is provided by Forrester et al. [42] and Forrester and Keane [43] and a general review of BO is given by Shahriari et al. [44]. For high-dimensional settings, Trust Region Bayesian Optimization (TuRBO) by Eriksson et al. [45] is widely used, and numerically stable EI variants such as Log Expected Improvement (LogEI) discussed by Ament et al. [46] address practical numerical issues that occur in acquisition evaluation and optimization.

Domain-specific studies demonstrate that BO is already used in composite forming contexts with simulation-generated data. Jagpal et al. [47] combined distributed magnetic clamping with BO in non-crimp-fabric preforming to reduce wrinkling. Chen et al. [48] applied GP surrogate modeling and BO to dry-fabric preform formability using simulation-generated data. More recently, Chen et al. [49] proposed a surrogate-modeling framework for high-dimensional forming optimization that combines GP-emulation, active-subspace dimension reduction, and sequential design to enable optimization with only tens of simulations. These contributions provide direct evidence that BO can deliver sample-efficient improvement in forming-related objectives under expensive simulation budgets.

1.3. Research gap and scope of this work

Although there is extensive work on simulation-driven parameter optimization, surrogate modeling, BO, and learning-based acceleration for composite forming, most approaches treat the actuation and constraint configuration as fixed and restrict optimization to a predefined set of process variables. Systematic strategies that leverage information learned during simulation-based optimization, for example surrogate-model structure or sensitivity information, to guide deliberate over-instrumentation of the forming setup, such as the targeted addition or placement of grippers, are not prominently addressed in the literature provided in Section 1.2. This creates a gap between optimizing within a chosen actuation concept and optimizing the actuation concept itself based on evidence gathered from expensive simulations.

To address this gap, this work investigates BO as a sample-efficient tool for minimizing out-of-plane wrinkling in the thermoforming of CoFRTP components. An overview of the real-world problem, its high dimensionality, and the associated optimization framework is provided in Section 2. The optimization problem is addressed using computationally expensive FEM simulations as the primary data generator (see Section 3). In Section 4, a set of BO strategies is introduced and benchmarked in Section 5 in a high-dimensional gripper-parameter space by comparing acquisition functions including Expected Improvement (EI) and Log Expected Improvement (LogEI), as well as the trust-region method Trust Region Bayesian Optimization (TuRBO), against a Sobol sampling baseline [50]. Using the data from the BO trials, a global sensitivity analysis based on the learned surrogate models is performed, providing insights into the influence of individual gripper parameters and their interactions on defect formation. Building on the optimized baseline configuration and these insights, an adjusted gripper configuration is investigated in Section 6, in which an additional gripper is introduced through over-instrumentation, enabling further improvements in forming quality with limited additional optimization effort.

2. Problem definition and optimization framework

This section provides an overview of the industrial-scale forming process for CoFRTPs and defines the optimization problem for the gripper parameters during forming. A quantitative wrinkling-related quality measure is introduced as the objective function. Finally, the optimization problem is formally stated together with practical constraints to ensure industrial relevance and computational tractability.

2.1. Industrial-scale forming process

The most established manufacturing process for CoFRTP components is the thermoforming of either organosheets or undulation-free tailored tape laminates produced from thermoplastic tapes [1]. In thermoforming, a pre-consolidated laminate consisting of differently oriented layers is first clamped into a gripper frame (see Fig. 1 (1)). This allows the laminate to be handled by a robot (see Fig. 1 (2)) between the different process stations and enables the application of tensile forces during forming. The laminate is subsequently transferred to an infrared oven (see Fig. 1 (4)), where it is heated to the initial forming temperature T_{init}, which lies above the melting temperature of the matrix polymer. In order to minimize cooling prior to forming, the heated laminate is then transferred to the press station within a short time frame (see Fig. 1 (3)). In the press, the laminate is deep-drawn into the temperature-controlled forming tool and subsequently cooled below the melting temperature.

To counteract the deformation behavior during thermoforming, tensile stresses can be introduced into the laminate by tensile grippers mounted on a gripper frame. It has been shown that increasing the number of tensile grippers while reducing the tensile force applied by each individual gripper can lead to a reduction in out-of-plane wrinkling [7,51]. The gripper positions and forces, depending on the tool geometry, material system, laminate layup, and process parameters, constitute a complex optimization problem aimed at minimizing out-of-plane wrinkling [52].

2.2. Gripper setup for the initial optimization problem

To investigate the optimization approach, the thermoforming of a quasi-isotropic laminate into the geometry shown in Fig. 2 was selected. The quasi-isotropic layup and the geometry, with its double-curved areas of varying degrees of curvature, both favor the forming defect out-of-plane wrinkling. The forming problem considered in this study therefore represents a realistic yet computationally tractable optimization challenge, ensuring that the investigated process parameters remain relevant for industrial applications while keeping the computational cost of the required forming simulations within reasonable limits. The used parametrizable gripper setup is shown in Fig. 2.

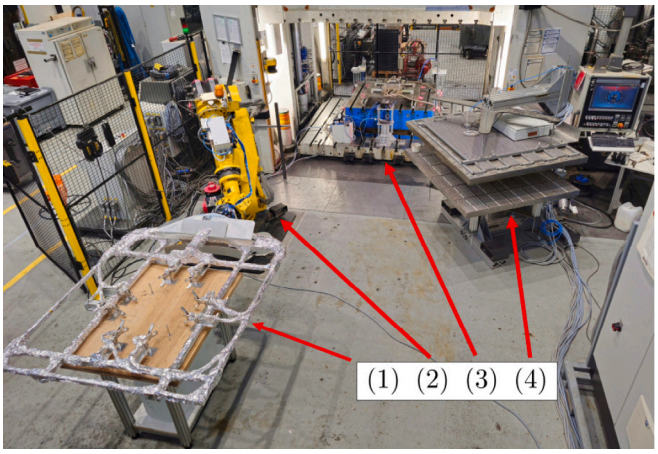

Fig. 1. Industrial-scale thermoforming process of CoFRTPs, adapted from Zeeb et al. [8]. (1) Gripper frame for clamping the laminate sheet; (2) robot for handling the gripper frame; (3) forming press; (4) infrared oven.

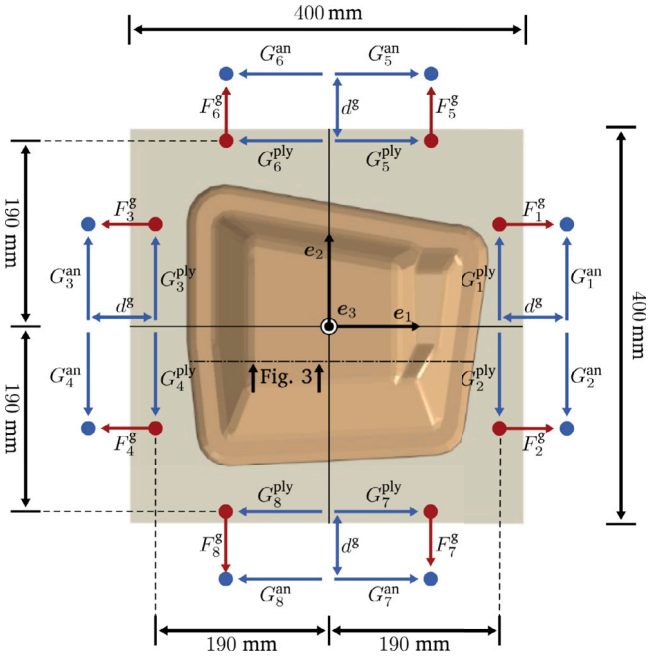

Fig. 2. Initial gripper configuration for the thermoforming process of CoFRTPs using eight grippers with space-fixed anchor points G_i^{an}, laminate-fixed needle points G_i^{ply}, and gripper forces F_i^g. The dashed line symbolizes the location of the cut-view from Fig. 3.

In the initial study, a total of eight grippers are utilized, with two grippers positioned along each edge of the laminate. Each gripper clamps the 400 mm × 400 mm laminate at the laminate fixed point G_i^{ply}, located 190 mm from the laminate center along the corresponding edge. The grippers are mounted to the gripper frame at their respective anchor points G_i^{an}, which are positioned at a distance d^g from the laminate boundary. The gripper force F_i^g is applied at the laminate-fixed point and is directed toward the corresponding anchor point G_i^{an}. The anchor point allows rotation about the axis e_3, enabling the tensile force to self-align with the laminate-fixed point along the material feed direction during the forming process. In this study, two gripper parameters are considered as design variables: the anchor position G_i^{an}

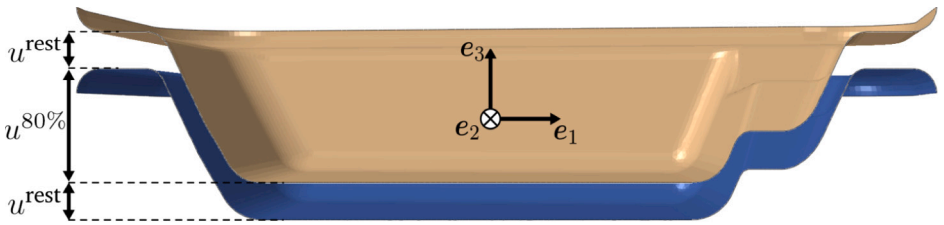

Fig. 3. Cross sectional side view of the tool geometry, including the upper tool position at 80% stroke used for the evaluation of the objective function. The location of the cut-view is indicated in Fig. 2.

and the gripper force F_i^{g}. All remaining process conditions are kept constant or are defined as dependent on G_i^{an} and F_i^{g}. As a result, a total of 16 optimization parameters are considered for the initial optimization problem. For notational convenience, the setting of the ith tensile gripper is represented by the tuple $\mathcal{G}_i^{\text{g}} := \left(G_i^{\text{an}}, F_i^{\text{g}}\right)$. Optimized gripper settings are indicated by a superscript $*$, e.g. $\mathcal{G}_i^{\text{g}*}$.

2.3. Global quality measure

To optimize the forming process, a quantitative quality measure is defined. For this purpose, the mean absolute curvature of the blanks is evaluated at an intermediate stage corresponding to 80% of the maximum tool stroke. Fig. 3 illustrates this evaluation point, together with the completed stroke $u^{80\%}$ and the remaining stroke u^{rest}. Only the blank's area between the forming tools is considered, as in practice, the material overhang is removed after forming. The choice of 80% stroke is empirical. For the present setup, this stage is considered representative because the wrinkle positions remain unchanged between 50% and 90% stroke, indicating that the relevant wrinkle pattern is already established by 80% stroke. In the final stage of the simulation, the tool increasingly flattens the geometry, which, in the present discretization, reduces the visibility of smaller wrinkles. This behavior is described in Appendix. The 80% stroke is therefore used as the evaluation point for the present optimization study. As a result, any reduction in the absolute curvature directly relates to a reduction in wrinkling of the blank.

The wrinkling indicator is formulated as a geometric quantity reconstructed from the deformed laminate surface. While curvature-related quantities are available directly from the FE model, they may exhibit pronounced element-wise variations, resulting in a non-smooth curvature field. A geometry-based formulation was therefore chosen, as it provides a smoother and more consistent representation of the wrinkle pattern, supports robust aggregation into a scalar objective, and can also be applied to experimentally measured surface data. Provided triangularized surface meshes for each ply in the blank, the principal curvatures κ_i^{I} and κ_i^{II} can be obtained at each node i of the mesh using the algorithm provided by Dong and Wang [53]. In the present implementation, the nodal curvature reconstruction is based on the one-ring neighborhood of each node i. Since the arithmetic mean would provide a disappearing curvature at saddle points with equal absolute but opposite principal curvatures, Haanappel [54] introduced the modified mean curvature

$$\bar{\kappa}_i = \frac{1}{2}\left(\left|\kappa_i^{\text{I}}\right| + \left|\kappa_i^{\text{II}}\right|\right). \tag{1}$$

The elemental modified mean curvature

$$\bar{\kappa}_k^{\text{el}} = \frac{1}{3}\sum_{j=1}^{3} \bar{\kappa}_{kj} \tag{2}$$

provides an element-wise curvature by averaging over the modified mean curvatures of nodes j for triangular element $k \in N_l^{\text{el}}$ [25]. Since the nodal curvatures are already reconstructed from the one-ring neighborhood of each node, this element-wise formulation introduces one additional local averaging step. In the present work, it was retained because it provided a smoother global wrinkling indicator than a direct nodal aggregation. The final objective function $\left\langle \bar{\kappa}^{\text{el}} \right\rangle$ is then obtained as an unweighted average of the element-wise modified mean curvature over all triangular elements of each ply and subsequently over all plies l.

$$\left\langle \bar{\kappa}^{\text{el}} \right\rangle = \frac{1}{L}\sum_{l=1}^{L} \frac{1}{N_l^{\text{el}}} \sum_{k=1}^{N_l^{\text{el}}} \bar{\kappa}_k^{\text{el}}. \tag{3}$$

Eq. (3) is minimized to globally reduce the amount and severity of out-of-plane wrinkles during forming.

The resulting scalar objective function Eq. (3) is intended as a global wrinkling indicator for ranking candidate process configurations within the present simulation and post-processing framework. It does not fully capture the spatial morphology of the wrinkle pattern. Different wrinkle patterns can therefore, in principle, lead to similar objective values if their overall contribution to the global curvature average is comparable. However, a global criterion was considered appropriate, as the objective is to reduce wrinkling across the entire formed part. A more localized objective would require prior weighting of specific regions and could otherwise incentivize the relocation of wrinkles rather than their overall reduction.

2.4. Optimization approach

Multiple studies have examined the effect of process parameters $\mathbf{x}$ on wrinkle formation $\left\langle \bar{\kappa}^{\text{el}} \right\rangle$ during the forming of CoFRPs [7,35,51]. However, the effect of process parameters and the grippers parameters can have different effects on the forming process depending on the geometry, material properties and layup configuration. Although existing FEM simulation models make it possible to model and test the influence of tensile grippers, this high-dimensional parameter space also makes simulation-assisted process optimization very time- and cost-intensive.

One possible baseline is to use a space-filling design (e.g., a grid or quasi-random sampling) and select the best evaluated configuration. In D_x dimensions, however, achieving a comparable per-parameter resolution requires a number of samples that scales on the order of $C(D_x)\cdot\xi^{D_x}$, where $C(D_x)$ is a constant dependent on the number of dimensions and ξ is the number of levels or samples per dimension. To achieve a high fidelity per-parameter resolution for the thermoforming simulation with $D_x = 16$, purely sampling methods become prohibitive. This effect is further amplified when the objective $\Omega(\mathbf{x}) = \left\langle \bar{\kappa}^{\text{el}} \right\rangle$ is highly sensitive to the inputs $\mathbf{x}$ or if strong parameter interactions dominate the response, then the required sampling spacing to reliably identify low-wrinkling regions decreases, which in turn increases the sample count even further. BO addresses these challenges by learning a surrogate model of the expensive objective from the available simulation data and using an acquisition function to adaptively allocate evaluations to regions that are both promising and uncertain. In this study, we aim to compare different BO strategies introduced in Section 4 to identify the most efficient approach for this high-dimensional problem. However, benchmarking multiple algorithms requires a substantial number of function evaluations to ensure statistical robustness. Conducting such a large volume of trials physically would be very expensive and time-consuming. Consequently, for the purpose of method development and

validation in this work, the physical forming process is substituted by the FEM simulation model described in Section 3. This allows for the generation of the necessary data to rigorously evaluate the optimization performance while maintaining a representation of the complex physical forming behavior.

3. Thermoforming simulation of the manufacturing process of CoFRTPs

Experimentally optimizing the forming process is time-consuming and costly. Numerical simulation therefore offers a cost-effective alternative for generating virtual process data and guiding the selection of process parameters. In this work, a thermoforming simulation model for CoFRTPs is employed to generate such virtual process data. The simulation model is implemented in the commercial FEM software Abaqus/Explicit and is based on the work of Dörr et al. [22,29]. The model follows an isothermal, layer-by-layer approach developed specifically for the thermoforming simulation of CoFRTPs. It captures the complex deformation behavior of CoFRTPs during thermoforming by accounting for both intra-ply and inter-ply mechanics. Specifically, the model features a decoupled membrane-bending formulation for the intra-ply response, rate-dependent material modeling of both membrane and bending behavior [22], and an isotropic inter-ply interaction formulation that accounts for non-penetration, adhesion, and sticking–sliding between adjacent plies [29]. The model has been experimentally validated for thermoforming of CoFRTPs with various laminate layups, including quasi-isotropic and biaxial configurations, with respect to wrinkle onset, wrinkle evolution, fiber reorientation, and material draw-in [22]. Comparisons between simulations and thermoforming experiments showed good agreement in deformation patterns, draw-in, and wrinkle formation for the investigated configurations. Based on this prior validation, the model is used here as a high-fidelity virtual data generator for simulation-driven optimization using BO. For a more in-depth discussion of the simulation model, the reader is referred to Dörr et al. [22,29].

3.1. Consideration of grippers in thermoforming simulation

Grippers are an essential component of the thermoforming process and significantly influence the wrinkling behavior of the formed part [5,6,8], necessitating their inclusion in the simulation model. The modeling strategy applied in this work builds on the methodology proposed by Poppe et al. [55]. This approach involves the use of a space-fixed anchor point G_i^{an}, which represents the bearing of the gripper on the gripper frame. Furthermore, a blank-fixed needle point G_i^{ply} is defined, representing the point on the blank where the material is clamped by a needle (see Fig. 2). Note that the needle point is not fixed in space but moves with the blank during forming. Due to the construction of the grippers, a small area around the needle point G_i^{ply} remains unheated during the heating phase, as the hardware blocks radiative heat transfer to this region, and the thermoplastic matrix in this localized area does not melt and therefore remains rigid during the forming process. To reflect this physical behavior in the simulation, a small cylindrical region around the needle point is defined, and all nodes through the thickness within this region are kinematically coupled to the needle point G_i^{ply}, thereby constraining their relative motion and accurately representing the rigid, clamped zone during forming. The gripper force F_i^{g} is applied as a concentrated force at the needle point and is always directed along the line connecting the anchor G_i^{an} and needle point G_i^{ply}. The correct direction of the gripper force is ensured by employing a one-dimensional translator element. An additional hinge element at the needle point G_i^{ply} allows rotational freedom of the ply about this point, enabling nodding motions of the gripper during forming.

3.2. Simulation model

The aforementioned thermoforming simulation model is employed to simulate the forming of a square blank into a complex double-curved geometry representative of an industrial component (see Fig. 2). The punch and die are modeled as rigid surfaces, and forming is applied in a displacement-controlled manner by prescribing a Dirichlet boundary condition on the punch, $u = 55.1\,\mathrm{mm}$, over a time period of $T = 1\,\mathrm{s}$. The laminate consists of four CoFRTP plies with an intrinsic thickness of $t_0 = 0.45\,\mathrm{mm}$ each, resulting in a total laminate thickness of $t = 1.8\,\mathrm{mm}$. The plies are oriented $[0°, 45°, 90°, -45°]$ relative to the e_1-axis (see Fig. 2). The initial blank dimensions are $400\,\mathrm{mm} \times 400\,\mathrm{mm}$, and the blank is discretized using 11 664 triangular elements per ply. Membrane and bending responses are decoupled by superimposing membrane (M3D3) and plate (S3) elements with shared nodes. Material behavior for the membrane response, bending response, and inter-ply interactions is implemented via user-defined subroutines in Abaqus/Explicit [22,23]. The interaction between the blank and the forming tools is modeled using a Coulomb friction formulation with a slip-rate- and pressure-dependent friction coefficient μ within the general contact framework of Abaqus/Explicit. Temperature effects are neglected due to the short process time, where temperature-driven effects are expected to have minimal influence on the forming behavior [56]. Therefore, isothermal conditions on the blank at 280°C are assumed throughout the forming process. Material parameters are based on in-house characterization of polyamide 6 reinforced with unidirectional carbon fibers (PA6-CF) at 280°C, following Dörr et al. [22,29].

Eight grippers are considered around the edges of the blank using the methodology described in Section 3.1. Each gripper applies a constant force F_i^{g} at the needle point G_i^{ply}, directed toward the corresponding anchor point G_i^{an}. To reduce the dimensionality of the optimization problem, the initial needle point locations are chosen to align with the anchor point locations, such that the initial force direction is orthogonal to the blank edge. During forming, the needle points move with the blank, whereas the anchor points remain fixed in space. This results in a total of 16 design variables: eight gripper forces F_i^{g} and eight anchor point locations G_i^{an}.

4. Gaussian process and Bayesian optimization

Optimizing the manufacturing process described in Section 2.1 presents a significant challenge as the objective function $\Omega(\mathbf{x}) = \langle \bar{\kappa}^{\mathrm{el}} \rangle$ representing the relationship between gripper parameters and the wrinkling quality metric (defined in Section 2.3), is computationally expensive to evaluate via FEM and lacks analytical gradients. This section outlines the GP surrogate model used to approximate the forming behavior and the BO acquisition functions that guide the search for optimal process parameters.

4.1. Gaussian processes

A GP is a distribution over functions, represented by a mean function $m(\cdot)$ and a covariance kernel $k(\cdot,\cdot')$. The mapping from the input space of gripper parameters $\mathbf{x} \in \mathcal{X}$ to the scalar wrinkling metric $\Omega(\mathbf{x})$ is approximated with $f(\mathbf{x}) \sim \mathcal{GP}(m(\mathbf{x}), k(\mathbf{x},\mathbf{x}'))$, where $m(\mathbf{x}) = \mathbb{E}[f(\mathbf{x})]$ and $k(\mathbf{x},\mathbf{x}') = \mathbb{E}\left[(f(\mathbf{x}) - m(\mathbf{x}))(f(\mathbf{x}') - m(\mathbf{x}'))\right]$ [57].

For an observed dataset $D = \{\mathbf{X}, \mathbf{y}\}$, where $\mathbf{X} = \{\mathbf{x}_n\}_{n=1}^N$ and $\mathbf{y} = \{f(\mathbf{x}_n)\}_{n=1}^N$ are the inputs and outputs of the observations, using GPs the observations can be expressed as a joint Gaussian distribution $f(\mathbf{X}) \sim \mathcal{N}(m(\mathbf{X}), k(\mathbf{X},\mathbf{X}'))$. The predictive distribution for a new point $\mathbf{x}$ is a Gaussian $\mathcal{N}(\mu_{f(\mathbf{x})}, \Sigma_{f(\mathbf{x})})$, where $\mu_{f(\mathbf{x})}$ represents the expected value and $\Sigma_{f(\mathbf{x})}$ the associated uncertainty (variance). The posterior mean and variance are derived by conditioning on the observed data [57] as

$$\begin{aligned} \mu_{f(\mathbf{x})} &= m(\mathbf{x}) + k(\mathbf{x},\mathbf{X})\,(k(\mathbf{X},\mathbf{X}))^{-1}\,(\mathbf{y} - m(\mathbf{X}))\,, \\ \Sigma_{f(\mathbf{x})} &= k(\mathbf{x},\mathbf{x}) - k(\mathbf{x},\mathbf{X})\,(k(\mathbf{X},\mathbf{X}))^{-1}\,k(\mathbf{X},\mathbf{x}) \end{aligned} \tag{4}$$

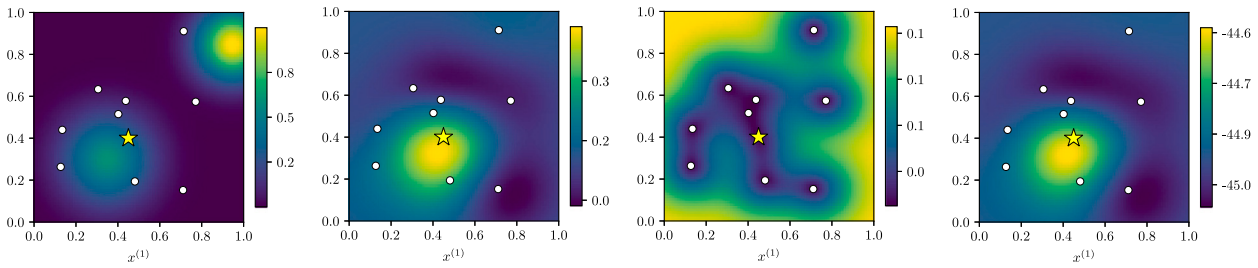

(a) Objective Ω (b) $\mathcal{GP}$ Mean $\mu_{f(\mathbf{x})}$ (c) $\mathcal{GP}$ StdDev $\Sigma_{f(\mathbf{x})}$ (d) LogEI($\mathbf{x}$)

Fig. 4. (a) Objective function Ω that is to be optimized over the input space $\mathbf{x} = (x^{(1)}, x^{(2)})$. White dots represent the observed data $\mathbf{y}$ at the input locations $\mathbf{X}$ and the yellow star represents the best observed output y_{best}. The global maximum is at $(0.95, 0.85)$ and there is one local maximum around $(0.35, 0.3)$. (b) $\mathcal{GP}$ predictive posterior mean $\mu_{f(\mathbf{x})}$. (c) Standard deviation $\sqrt{\Sigma_{f(\mathbf{x})}}$ of a GP. (d) LogEI over the input domain $\mathcal{X}$ conditioned on the observed data $D = \{\mathbf{X}, \mathbf{y}\}$ for a constant mean function and a RBF kernel.

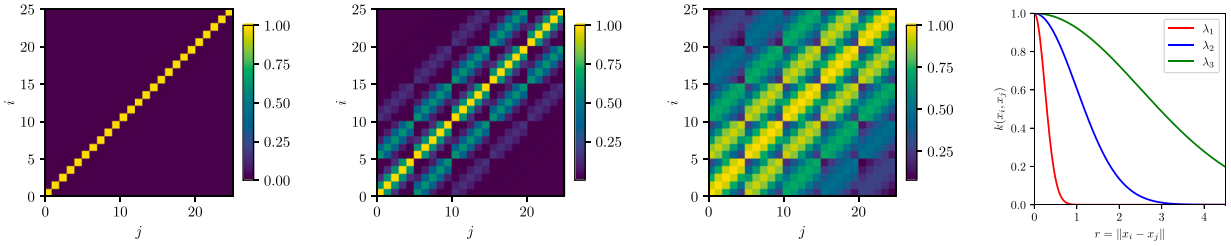

(a) $\boldsymbol{\lambda}_1 = (0.25, 0.25)$ (b) $\boldsymbol{\lambda}_2 = (1.0, 1.0)$ (c) $\boldsymbol{\lambda}_3 = (2.5, 2.5)$ (d) r vs $k(\mathbf{x}_i, \mathbf{x}_j)$

Fig. 5. Visualization of RBF kernel behavior for different lengthscales evaluated for 25 evenly spaced out input points $\mathbf{X}$ in the input space with $D_x = 2$. (a), (b), and (c) represent the covariance matrix $\mathbf{K} = k(\mathbf{X}, \mathbf{X})$ using the RBF kernel with different lengthscales λ. Small value of λ leads to more localized correlation and larger value of λ helps in learning correlation between distant input locations as well. (d) Decrease in correlation between two input locations with distance for different λ values.

The hyperparameters of the kernel, such as lengthscales, are typically estimated by maximizing the marginal log-likelihood of the observed data. Fig. 4 shows the learned predictive posterior mean and standard deviation of a Gaussian process conditioned on the observed data for a constant mean function and a Radial Basis Function (RBF) kernel.

A standard choice is the RBF kernel with Automatic Relevance Determination (ARD), which assigns an independent lengthscale $\lambda^{(d)}$ to each input dimension d defined as

$$k(\mathbf{x}, \mathbf{x}') = \exp\left(-\frac{1}{2} \sum_{d=1}^{D_x} \frac{(x^{(d)} - x'^{(d)})^2}{(\lambda^{(d)})^2} \right),$$

where D_x is the dimensionality of the input space (see Fig. 5). However, as dimensionality D_x increases, the Euclidean distance between points grows, often leading to poor model performance if standard lengthscale priors are used [58]. The "vanilla" priors typically do not account for this geometric expansion, causing the model to underestimate correlations. To mitigate this, the dimension-aware priors proposed by Hvarfner et al. [58] are adopted. By scaling the lengthscale prior with the dimensionality, the posterior is prevented from collapsing to small values where no correlation is learned. The scaled log-normal prior is given by $\log \lambda^{(d)} \sim \mathcal{N}(\mu_0 + \frac{1}{2} \log D_x, \sigma_0^2)$, for each dimension $d = 1, \ldots, D_x$ [58]. This simple adjustment significantly improves the robustness of the surrogate model in high-dimensional settings, enabling standard acquisition functions to perform effectively.

4.2. Bayesian optimization

BO is a sequential decision making approach under uncertainty. It uses the GP's posterior distribution to sequentially select the next input configuration $\mathbf{x}_{\text{next}}$ to evaluate. This decision is guided by an acquisition function that balances exploration and exploitation to find the optimal solution. Three specific strategies commonly used in BO are introduced and later evaluated in Section 5.

4.2.1. Expected Improvement (EI)

The Expected Improvement (EI) strategy selects the point that maximizes the expected improvement over the current best observed value y_{best}, defined as $\text{EI}(\mathbf{x}) = \mathbb{E}_{p(y|\mathbf{x},D)}\left[\max\left(0, y - y_{\text{best}}\right)\right]$ [59]. Given the Gaussian predictive distribution $f(\mathbf{x}) \sim \mathcal{N}(\mu_{f(\mathbf{x})}, \Sigma_{f(\mathbf{x})})$ as mentioned in Eq. (4), EI can be computed in closed form using the standard normal probability density function (PDF) ϕ and cumulative distribution function (CDF) Φ as

$$\text{EI}(\mathbf{x}) = \sqrt{\Sigma_{f(\mathbf{x}_{\text{next}})}}\, h\left(\frac{\mu_{f(\mathbf{x}_{\text{next}})} - y_{\text{best}}}{\Sigma_{f(\mathbf{x}_{\text{next}})}} \right), \quad h(a) = \phi(a) + a\,\Phi(a). \tag{5}$$

EI is a standard and robust acquisition function. However, EI tends to become numerically zero beyond the best observed region. This causes EI to focus primarily on exploitation around the best observed value so far, i.e., the current local maximum. Since it becomes negligible in regions with low predicted improvement, it lacks sufficient exploratory bias and may fail to identify optima beyond the initially discovered local optimum.

4.2.2. Log Expected Improvement (LogEI)

To overcome the numerical limitations of standard EI, Ament et al. [46] introduced LogEI, which computes the logarithm of the expected improvement. By using a numerically stable formulation, LogEI maintains non-zero gradients even in regions where the improvement is infinitesimal

$$\mathbf{x}_{\text{next}} = \arg\max_{\mathbf{x} \in \mathcal{X}} \text{LogEI}(\mathbf{x}); \quad \text{LogEI}(\mathbf{x}) = \log h(a) + \log \sqrt{\Sigma_{f(\mathbf{x}_{\text{next}})}}. \tag{6}$$

The implementation utilizes a piecewise formulation (as detailed in 46) to ensure precision across all values of a. This allows the optimizer to continue making progress and refining the solution in areas where standard EI would effectively vanish, providing a better balance between exploration and exploitation. Fig. 4(d) shows the LogEI over the input domain $\mathcal{X}$ conditioned on the observed data D for a constant

mean function and a RBF kernel. It can be observed that LogEI is not zero beyond the region best observed region and it can explore around the boundary as well. LogEI is zero only around the locations it has observed. This ensures a better exploration–exploitation trade-off.

4.2.3. Trust Region Bayesian Optimization (TuRBO)

To further tackle the challenges of high-dimensional optimization, Trust Region Bayesian Optimization (TuRBO) [45] is employed. Unlike standard BO which uses a single global GP, TuRBO maintains one or more local Trust Regions (TRs) centered around the best solutions found so far. A local GP is trained within each TR, and candidates are generated via Thompson Sampling. The size of the TR is dynamically adjusted. A successful step is defined as a step that improves the best observed value y_{best}. After consecutive successful steps, the TR is expanded by a factor of two and after consecutive failures, it is shrunk by half. This local approach allows TuRBO to model the objective function more accurately in the relevant regions of the search space, typically leading to faster convergence for complex, high-dimensional engineering problems. Algorithm 1 summarizes the TuRBO algorithm as proposed by Eriksson et al. [45].

Algorithm 1: TuRBO Algorithm for B TRs and sequential BO

Input: Objective Ω, hyperparameters $\tau_{\text{succ}}, \tau_{\text{fail}}, L_{\min}, L_{\max}, L_{\text{init}}$
Output: Best solution found
Initialize B TRs with random samples $\mathcal{D}^{(b)}$;
while *not converged* **do**
  for $b = 1, \ldots, B$ **do**
    Update $\mathcal{TR}^{(b)}$ center and size $L^{(b)}$ based on success/failure counts;
    Train local $\mathcal{GP}^{(b)}$ on $\mathcal{D}^{(b)}$ within $\mathcal{TR}^{(b)}$;
    Select candidate $\mathbf{x}_{\text{next}}^{(b)}$ via Thompson sampling on $\mathcal{GP}^{(b)}$;
    Evaluate $y_{\text{next}}^{(b)} \leftarrow \Omega(\mathbf{x}_{\text{next}}^{(b)})$ and update $\mathcal{D}^{(b)}$;
    Update success/failure counters based on improvement over best;
  end
  Update global best solution $\mathbf{x}_{\text{best}}$ if improved;
end

The selection of the center of a TR in TuRBO is a greedy method of choosing the best observed point so far. Namura and Takemori [60] discuss that it can lead to suboptimal performance when TRs collapses. To avoid them from collapsing to a local minima, they proposed to use Regional Expected Improvement (REI) to select a new center when the length of the TR becomes smaller than the threshold $L_{\min}$. REI is defined as the expectation of EI over a Trust Region $\mathcal{TR}$. The center of the $\mathcal{TR}$ is chosen as the point in the input domain $\mathcal{X}$ that maximizes the REI. Formally, it is defined as

$$\text{REI}(\mathbf{x}) = \frac{1}{V_{\mathcal{TR}}} \int_{\mathcal{TR}} \text{EI}(\mathbf{x}) d\mathbf{x} \approx \frac{1}{N_{\mathbf{x}}} \sum_{i=1}^{N_{\mathbf{x}}} \text{EI}(\mathbf{x}_i), \tag{7}$$

where $V_{\mathcal{TR}}$ is the volume of $\mathcal{TR}$, $\text{EI}(\mathbf{x})$ is the expected improvement at the point $\mathbf{x}$, as mentioned in Eq. (5), and $N_{\mathbf{x}}$ is the number of Monte Carlo samples within $\mathcal{TR}$.

5. Bayesian optimization of the initial gripper configuration on virtual process data

This section presents the optimization of the initial gripper positions and forces using the BO methods described in Section 4.2. The optimization aims to minimize wrinkle formation during the simulated thermoforming process, using the numerical model described in Section 3. Subsequently, an ARD lengthscale based sensitivity analysis is performed using the learned Gaussian process surrogate models.

5.1. Numerical test setup

The simulations were performed using the numerical setup as described in Section 3. The optimization process considers a 16-dimensional input space, consisting of 8 gripper positions G_i^{an} and 8 associated force parameters F_i^g. To avoid overlap, the gripper positions were constrained such that each gripper was restricted to a non-overlapping segment of its assigned sheet edge. The gripper forces pulling on the sheet were limited to 20–200 N, representing the practical force range of the physical gripper system [8,52]. The region of interest for optimization was taken as the cut-out portion of the laminate plies, corresponding to the projection of the forming tool (Fig. 2). The corresponding objective function Eq. (3) was implemented as described in Section 2.3.

The input parameter optimization consists of two sequential steps. First, the input parameter space is explored using 32 Sobol samples [50] in order to initialize the GP. Next BO was performed for up to 150 iterations in total, including the initial sampling iterations which were kept the same across the different BO methods. The applied methods consist of EI, LogEI, and TuRBO (Section 4.2) as well as Sobol sampling [50] for baseline comparison. These numerical experiments were repeated three times each. The observed performance trends were consistent across all runs. However, due to the significant computational cost of the 16-dimensional optimization problem, the number of repetitions was limited to three, which does not permit a statistically rigorous significance analysis.

5.2. Results of the Bayesian optimization procedures on the initial gripper configuration

The resulting curvature field distributions for the different optimization methods are presented in Fig. 7, while the convergence behavior is illustrated in Fig. 6. A reference geometry with strongly reduced wrinkle formation is included for contextual comparison (Fig. 7(a)), whereas randomly sampled gripper positions and forces (Fig. 7(b)) serve as a baseline. The reference geometry is obtained by forming a blank consisting of only two plies with perpendicular fiber orientations $[0°, 90°]$. This laminate configuration allows deformation to occur primarily through in-plane shear, as no shear-stiffening ±45° plies are present. As a result, the reference does not represent an achievable optimum for the investigated laminate, but rather provides a lower bound on wrinkle formation under more favorable material conditions.

All optimization methods demonstrated the ability to reduce wrinkle formation; however, their convergence behavior and final performance differed significantly. Overall, LogEI and TuRBO (Fig. 7(e), (f)) showed strong performance, whereas Sobol sampling and EI (Fig. 7(c), (d)) achieved only marginal improvements over the best initially sampled configurations (Fig. 6). Across the three experimental runs per BO method, LogEI performed marginally better than TuRBO, which terminated early after 118 iterations due to its automatic stop criterion. In contrast, EI was unable to outperform even the baseline Sobol sampling approach. Despite the overall improvement in curvature performance, all optimized configurations exhibited persistent wrinkle formation along the left and top boundaries of the region of interest (Fig. 7), indicating that local defect mitigation in these critical areas remains challenging and may require further refinement of the gripper setup or additional process controls. Nevertheless, the optimized geometries clearly outperform both the random baseline (Fig. 7(b)) and the best configuration obtained from Sobol sampling (Fig. 7(c)). The reported solutions correspond to the best configurations identified within the available optimization budget and do not imply any guarantees of global optimality.

Each iteration consists of two phases, the simulation step and the subsequent BO step, which includes evaluation of the simulation results, updating of the BO model, and selection of the next input. Across all three experimental runs optimizing eight grippers, the simulation

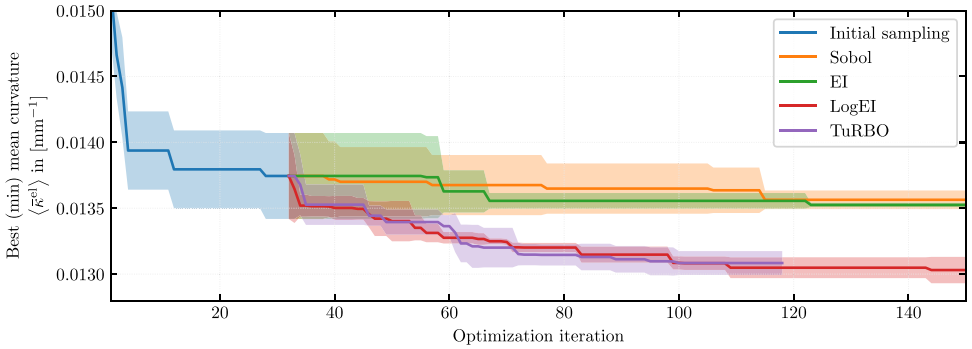

Fig. 6. Visualization of mean ± standard deviation of blank minimum mean curvatures up to each optimization iteration. For the first 32 iterations inputs were sampled using Sobol sampling. Consecutive iterations depict the three different applied BO-Methods as well as Sobol sampling. TuRBO stops early due to its automatic stop criterion.

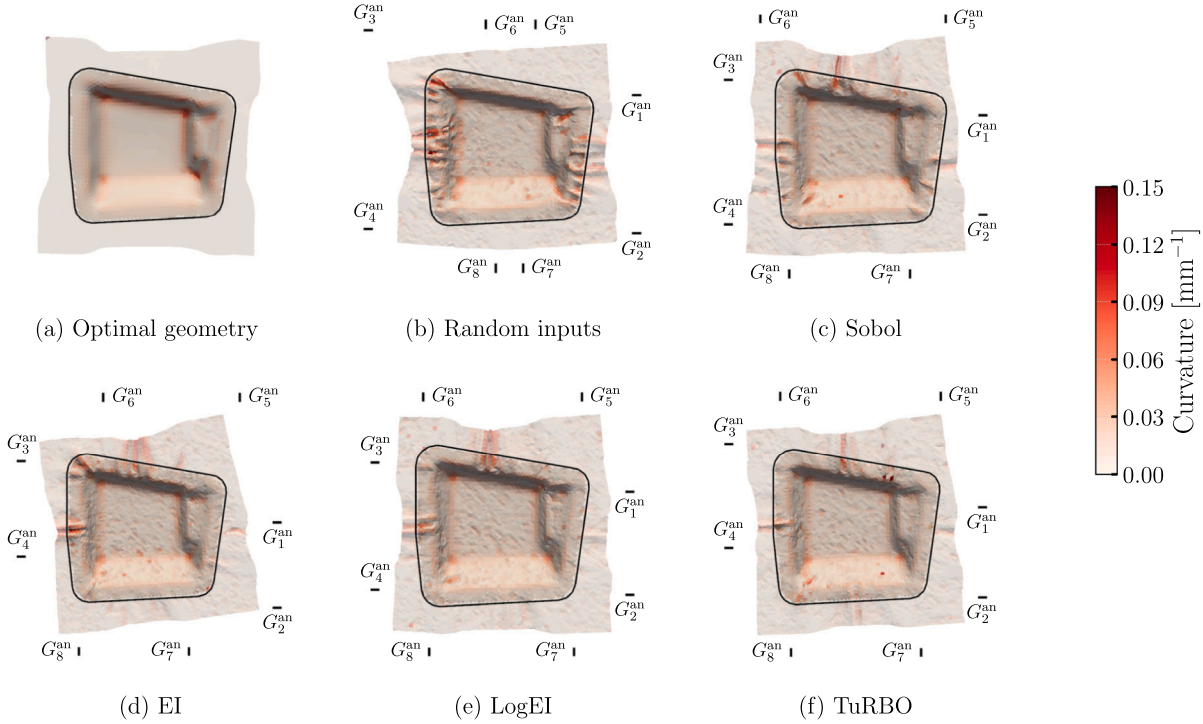

Fig. 7. Simulation results with element wise curvatures for: (a) Reference geometry with reduced wrinkle formation under altered laminate conditions ($\langle \bar{\kappa}^{el} \rangle$ = 0.00995 mm^{-1}). (b) Randomly sampled gripper forces and positions ($\langle \bar{\kappa}^{el} \rangle$ = 0.01597 mm^{-1}). Best result after 150 iterations for (c) Sobol ($\langle \bar{\kappa}^{el} \rangle$ = 0.01366 mm^{-1}), (d) EI ($\langle \bar{\kappa}^{el} \rangle$ = 0.01355 mm^{-1}), (e) LogEI ($\langle \bar{\kappa}^{el} \rangle$ = 0.01291 mm^{-1}), (f) TuRBO ($\langle \bar{\kappa}^{el} \rangle$ = 0.01300 mm^{-1}). The black contour outlines the forming tool as well as the optimized geometry. The black bars indicate the gripper's respective anchor points.

step took 1230 ± 269 s (mean ± standard deviation) on average, while the BO step required 9.18 ± 0.77 s (mean ± standard deviation) on average. It becomes apparent that the simulation step is the limiting factor, even for the relatively coarse mesh used in these experiments. The total optimization runtime amounted to 40.65 ± 8.51 h (mean ± standard deviation) on average for a budget of 150 iterations (including TuRBO, which did not use all 150 iterations), of which the first 32 were performed in parallel as part of the initial sampling. Each experiment was conducted on 8 CPU cores of an AMD EPYC 9454 processor.

Fig. 8 summarizes the lengthscales $\lambda^{(d)}$ learned by the GP surrogate models using ARD as introduced in Section 4. Within the chosen kernel and model assumptions, smaller lengthscales indicate a stronger influence of the corresponding input dimension on the GP predictions. A small learned lengthscale $\lambda^{(d)}$ corresponds to rapid variation of the function along the dth input dimension, meaning that small changes in this input lead to significant changes in the predicted output and therefore indicate a high sensitivity with respect to that dimension. The box plot shows the distribution of the learned lengthscales for each input dimension across the different optimization runs. The results indicate that the surrogate models are generally more sensitive to gripper position parameters than to gripper force parameters.

6. Over-instrumentation of the gripper configuration

To further improve the forming quality in the thermoforming process, the potential of adding additional grippers to the existing gripper configuration is investigated. Specifically, a guided over-instrumentation approach is performed in which an additional gripper is introduced without restarting the optimization from scratch, but instead leveraging the solution previously obtained in the 16-dimensional optimization domain. Regional Expected Improvement (REI), defined as the expectation of EI over a Trust Region (TR), is employed to

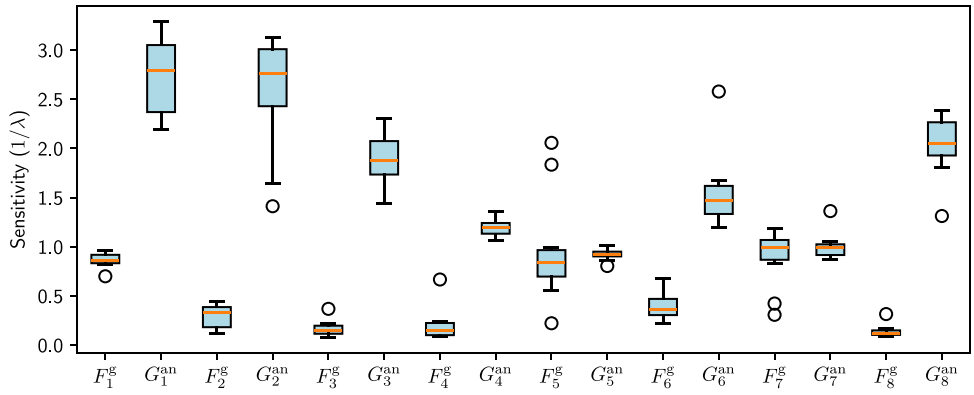

Fig. 8. ARD-based sensitivity analysis of the gripper parameters $\mathcal{G}_i^g = (G_i^{an}, F_i^g)$ using the learned Gaussian process surrogate models with a squared exponential kernel. The box plot shows the distribution of the lengthscales for each input dimension over the different BO runs.

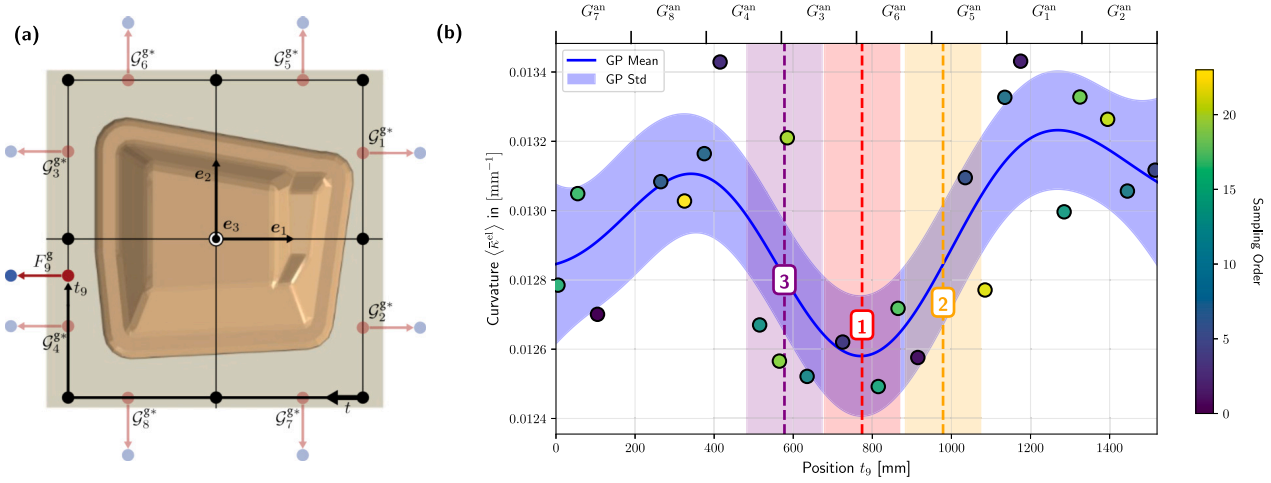

Fig. 9. (a) One-dimensional exploration of the result space by introducing an additional ninth gripper $\mathcal{G}_9^g$ (b) Visualization of a mean and variance of a Gaussian process fit to 24 samples of the geometry's mean curvature for varying positions of a ninth gripper, where all other inputs are constant. The samples are obtained through FEM simulations and displayed as colored dots, where the color indicates the sampling order. The corresponding gripper positions are shown above the graph. The three highest-scoring, non-overlapping TRs are highlighted as vertical colored bands.

guide the selection of the additional gripper position. The REI of the additional gripper provided by the model can than be used to support the process engineer in identifying promising regions for the additional gripper. This section describes the modifications applied to the gripper configuration, the rationale underlying these adjustments, the guided procedure used to identify promising locations for an additional gripper, and the results obtained by applying BO to the locally adapted configuration. The results demonstrate that guided over-instrumentation, despite the lack of formal optimality guarantees, can achieve substantial improvements in forming quality with comparatively low additional effort.

6.1. Domain reduction for efficient optimization

The BO applied to the initial gripper configuration proved effective in reducing wrinkle formation for this complex black-box problem with a high-dimensional input space. In particular, advanced optimization strategies such as LogEI and TuRBO achieved faster convergence and greater wrinkle reduction than standard EI and Sobol sampling, as shown in Fig. 6. However, both LogEI and TuRBO reached a plateau in the objective function value after a certain number of iterations. While further improvements might still be possible by continuing the optimization, larger gains are expected from modifying the gripper configuration itself by introducing additional grippers. This is especially relevant in industrial applications, where adding an additional gripper may be feasible in terms of cost and complexity, but identifying the most effective placement is nontrivial, as it introduces new design parameters that must be optimized. Moreover, while adding grippers in physical experiments is costly and complex, it is straightforward to implement and evaluate alternative configurations in simulation.

In the following, an adjusted gripper configuration is considered in which the previously optimized gripper settings are kept fixed and a single additional gripper is introduced. For the initial configuration, the setting of the ith gripper is described by the tuple $\mathcal{G}_i^g = \left(G_i^{an}, F_i^g\right)$ with $i \in \{1, \dots, 8\}$. Based on the previously obtained optimum, these grippers are fixed at their optimized settings $\mathcal{G}_i^{g*} = \left(G_i^{an*}, F_i^{g*}\right)$. An additional ninth gripper with setting $\mathcal{G}_9^g = \left(G_9^{an}, F_9^g\right)$ is then introduced. During this exploratory phase, the force F_9^g is kept constant, and the anchor position G_9^{an} is parameterized by the arc length $t \in [0, 1520)$ mm along the laminate boundary. As a result, the exploration of potential gripper locations constitutes a one-dimensional sampling problem which is visualized in Fig. 9. A GP surrogate model is then fitted to 24 Sobol sampled data points, and REI is used to propose centers for the top three non-overlapping TRs as shown in Section 4.2.3. The width of each TR is chosen as 190 mm based on process expertise, such that each region represents a practically relevant portion of the laminate edge. These regions serve as guidance for identifying locations where adding an additional gripper is most likely to yield further reductions in wrinkle formation. The analysis indicates that the upper left region

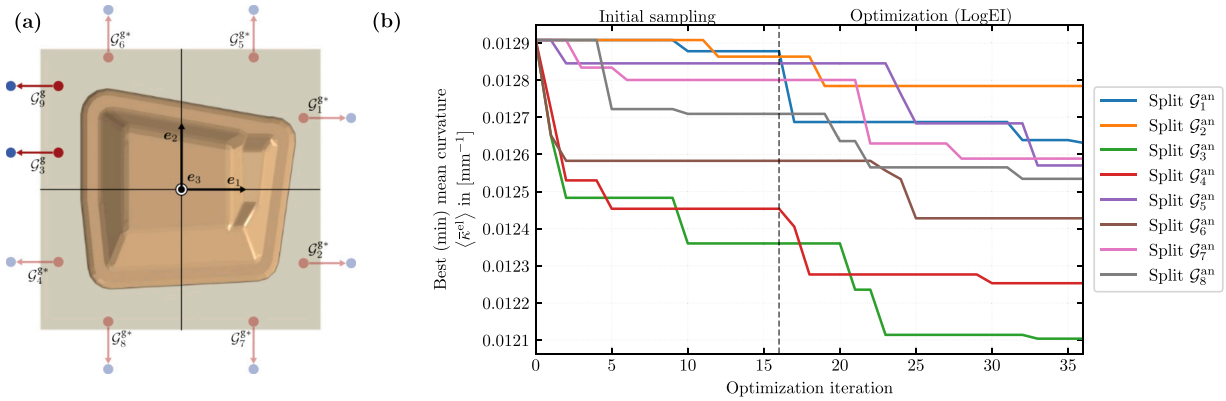

Fig. 10. Adjusted gripper configuration in which an additional gripper $\mathcal{G}_9^g$ is introduced on a selected edge. The gripper $\mathcal{G}_9^g$ and the gripper parameters $\mathcal{G}_i^g$ on this edge are optimized. (b) Visualization of blank minimum mean curvatures at each iteration for the 4 dimensional optimization of every split gripper pair. For the first 16 iterations inputs were sampled using Sobol sampling. Consecutive iterations depict the optimization via LogEI.

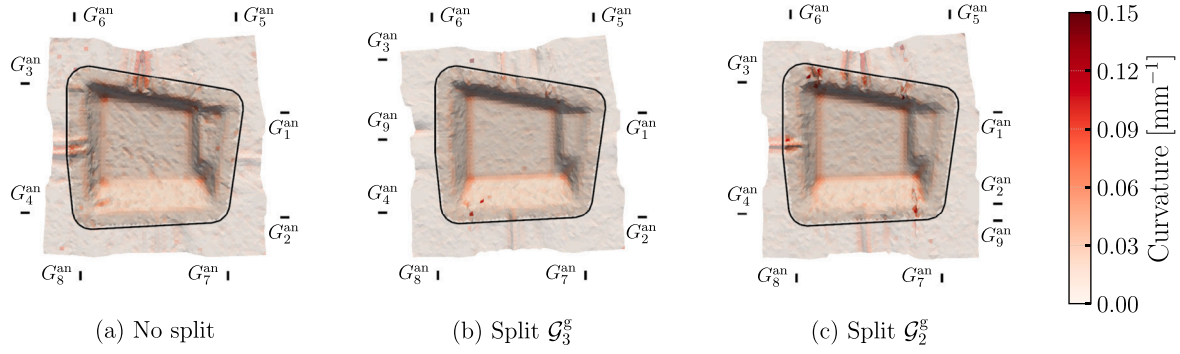

Fig. 11. Simulation results with element-wise curvatures for: (a) the optimized geometry obtained with the initial eight-gripper configuration ($\langle \bar{\kappa}^{el} \rangle$ = 0.01291 mm^{-1}); (b) the best result obtained after guided over-instrumentation, where an additional gripper $\mathcal{G}_9^g$ is introduced and locally optimized near $\mathcal{G}_3^g$ ($\langle \bar{\kappa}^{el} \rangle = 0.01210$ mm^{-1}); (c) the least effective result obtained after introducing $\mathcal{G}_9^g$ near $\mathcal{G}_2^g$ ($\langle \bar{\kappa}^{el} \rangle = 0.01278$ mm^{-1}).

of the geometry, corresponding to the anchor locations of grippers $\mathcal{G}_4^g$, $\mathcal{G}_3^g$, $\mathcal{G}_6^g$, and $\mathcal{G}_5^g$, is particularly promising. In practice, the number and width of TRs can be chosen arbitrarily. Reducing the area that is subject to further optimization reduces computational effort but limits the potential gain in quality obtained from further optimization.

6.2. Bayesian optimization on the locally adjusted gripper configuration

Further optimization can be streamlined by only considering grippers with domains within the identified promising regions. One at a time each of these grippers $\mathcal{G}_i^{g*}$ on the selected edge is replaced by two grippers $\mathcal{G}_i^g$ and $\mathcal{G}_9^g$, allowing for a redistribution of both positions and forces along the corresponding edge section. All other grippers remain fixed at their previously optimized settings. As a result, the local optimization problem becomes four-dimensional, consisting of two anchor positions and two gripper forces associated with the split gripper pair. The position domain of the original gripper is divided into two equal subdomains, and the admissible force range is split accordingly to avoid excessive force imbalance. Each locally adjusted gripper configuration is optimized using LogEI, initialized with 16 Sobol samples and followed by up to 20 consecutive BO steps (see Fig. 10).

The best optimization results are obtained when locally augmenting the gripper configuration in the vicinity of gripper $\mathcal{G}_3^g$, followed by the regions associated with $\mathcal{G}_4^g$ and $\mathcal{G}_6^g$. These findings are consistent with the promising regions identified during the one-dimensional exploration phase shown in Fig. 9. Most optimizations plateau after only 10 BO iterations, indicating a rapid stabilization of the objective value.

The best result of 0.01210 mm^{-1} represents a substantial improvement over the best eight-gripper configuration, which achieved a minimum mean curvature of 0.01291 mm^{-1}. The improvement of 0.00081 mm^{-1} obtained by introducing a single additional gripper $\mathcal{G}_9^g$ and locally optimizing only four parameters is comparable to the improvement achieved during the original 16-dimensional optimization. This improvement is also evident in the resulting geometry shown in Fig. 11, where the optimized configuration with the additional gripper $\mathcal{G}_9^g$ located near $\mathcal{G}_3^g$ is largely free of pronounced wrinkles. The results empirically demonstrate that the use of REI can be an effective strategy for methodical over-instrumentation in manufacturing processes. The results also show the connection of the Bayesian optimization methods as not just a black-box optimization tool, but a tool that can be used to support the process engineer in the identification of promising regions for the over-instrumentation. Overall, the results indicate that guided over-instrumentation combined with local re-optimization is an effective strategy for further improving forming quality with limited additional optimization effort.

It should be noted that the present over-instrumentation study addresses only a restricted concept modification, namely the targeted addition of a single gripper while keeping the remaining actuation concept fixed. More general concept level optimization could additionally consider variables such as the number and type of grippers or parameterized time dependent force, path, or stroke strategies. In principle, the present BO based framework could be extended to such settings by introducing hybrid design variables and suitable parameterizations of time dependent controls, which is beyond the scope of this work.

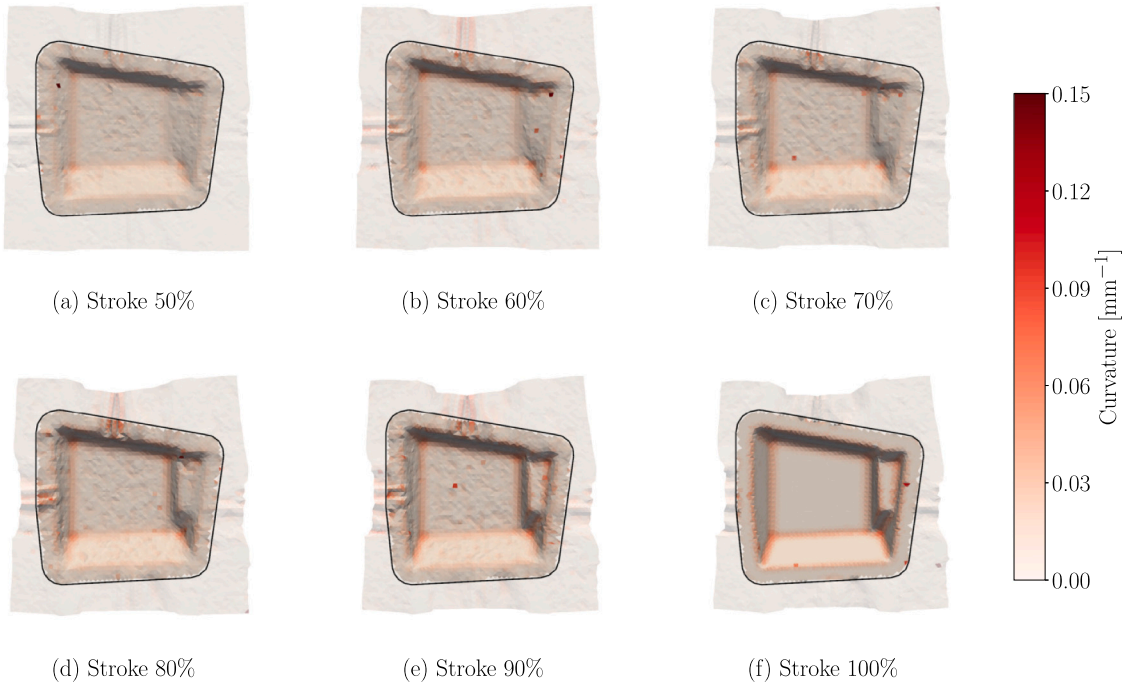

Fig. A.12. Wrinkle formation at different stroke lengths. The wrinkle positions remain unchanged from 50% to 90% stroke, while full tool closure increasingly flattens the geometry in the simulation.

7. Conclusion and outlook

This work investigated the application of Bayesian Optimization (BO) for optimizing process settings, specifically gripper positions and forces, in the thermoforming of continuous fiber-reinforced thermoplastics. The optimization was based on computationally expensive FEM simulations, requiring the use of sample-efficient optimization strategies. Advanced state-of-the-art BO methods, including Log Expected Improvement (LogEI) and Trust Region Bayesian Optimization (TuRBO), demonstrated superior performance compared to standard Expected Improvement (EI) and Sobol sampling, achieving substantial reductions in wrinkle formation with fewer simulation evaluations. The optimization reached a performance plateau after a certain number of iterations, indicating that further improvements could not be achieved by tuning the existing gripper parameters alone. To overcome this limitation, an over-instrumentation approach was introduced, in which the gripper configuration was modified by adding an additional gripper at strategically selected locations. Guided by a one-dimensional exploration of candidate positions, this approach enabled targeted local re-optimization without restarting the full high-dimensional optimization. Applying BO to the adjusted gripper configuration confirmed that guided over-instrumentation leads to further improvements in forming quality with limited additional optimization effort. In particular, the results show that locally increasing actuation at selected edges can effectively mitigate residual wrinkling that cannot be eliminated by the initial gripper configuration. Overall, the findings highlight the potential of BO for optimizing complex manufacturing processes and demonstrate how strategic over-instrumentation can extend the performance limits of existing process configurations.

Building on the guided concept adaptation considered in the present study, future research should extend the framework to richer design variables, such as gripper number and type and parameterized time-dependent actuation or stroke strategies. These extended optimization strategies should then be validated in experimental forming trials to assess their robustness beyond simulation. In this context, a combined simulation–experimental workflow could be explored, where BO is first used to pre-explore the parameter space in simulation and the most promising configurations are subsequently refined experimentally, thereby reducing the number of costly physical trials.

CRediT authorship contribution statement

Frank Doehner: Writing – review & editing, Writing – original draft, Visualization, Validation, Software, Methodology, Investigation, Formal analysis, Data curation, Conceptualization. **Johannes Mitsch:** Writing – review & editing, Writing – original draft, Visualization, Validation, Software, Methodology, Investigation, Formal analysis, Data curation, Conceptualization. **Saksham Kiroriwal:** Writing – review & editing, Writing – original draft, Visualization, Validation, Software, Methodology, Formal analysis, Data curation, Conceptualization. **Shahenda Youssef:** Writing – review & editing, Writing – original draft, Visualization, Validation, Software, Methodology, Investigation, Formal analysis, Data curation, Conceptualization. **Georg Zeeb:** Writing – review & editing, Writing – original draft, Validation, Methodology, Investigation, Conceptualization. **Frank Henning:** Writing – review & editing, Supervision, Funding acquisition. **Luise Kärger:** Writing – review & editing, Supervision, Funding acquisition, Conceptualization. **Jürger Beyerer:** Writing – review & editing, Supervision, Funding acquisition, Conceptualization.

Declaration of competing interest

The authors declare that they have no known competing financial interests or personal relationships that could have appeared to influence the work reported in this paper.

Acknowledgments

This work is part of the DFG AI Research Unit 5339 (project no. 459291153) funded by the Deutsche Forschungsgemeinschaft (DFG,

German Research Foundation) to accelerate maturation of immature manufacturing processes. The authors acknowledge support by the state of Baden-Württemberg through bwHPC.

Appendix. Wrinkle evolution at different tool strokes

The evolution of the wrinkle pattern at different tool strokes is illustrated in Fig. A.12 for the present simulation setup. The comparison shows that the wrinkle positions remain unchanged from 50% to 90% stroke, indicating that the relevant wrinkle pattern is already established at intermediate stages of the forming process. At full tool closure, the geometry is increasingly flattened, which reduces the visibility of smaller wrinkles in the present discretization. This supports the use of the 80% stroke stage as the evaluation point for the objective function in the optimization study.

Data availability

Data will be made available on request.

References

[1] Henning F, Kärger L, Dörr D, Schirmaier FJ, Seuffert J, Bernath A. Fast processing and continuous simulation of automotive structural composite components. Compos Sci Technol 2019;171:261–79. http://dx.doi.org/10.1016/j.compscitech.2018.12.007.

[2] Krueger R, Bergan A. Advances in thermoplastic composites over three decades – A literature review. 2024, URL: https://ntrs.nasa.gov/citations/20240005376.

[3] Vanclooster K, van Goidsenhoven S, Lomov SV, Verpoest I. Optimizing the deepdrawing of multilayered woven fabric composites. Int J Mater Form 2009;2(1):153. http://dx.doi.org/10.1007/s12289-009-0522-9.

[4] Lessard H, Lebrun G, Benkaddour A, Pham X-T. Influence of process parameters on the thermostamping of a [0/90]12 carbon/polyether ether ketone laminate. Compos Part A: Appl Sci Manuf 2015;70:59–68. http://dx.doi.org/10.1016/j.compositesa.2014.12.009.

[5] Breuer U, Neitzel M, Ketzer V, Reinicke R. Deep drawing of fabric-reinforced thermoplastics: Wrinkle formation and their reduction. Polym Compos 1996;17(4):643–7. http://dx.doi.org/10.1002/pc.10655.

[6] Harrison P, Gomes R, Curado-Correia N. Press forming a 0/90 cross-ply advanced thermoplastic composite using the double-dome benchmark geometry. Compos Part A: Appl Sci Manuf 2013;54:56–69. http://dx.doi.org/10.1016/j.compositesa.2013.06.014.

[7] Schug A, Winkelbauer J, Hinterhölzl R, Drechsler K. Thermoforming of glass fibre reinforced polypropylene: A study on the influence of different process parameters. AIP Conf Proc 2017;030010. http://dx.doi.org/10.1063/1.5007997.

[8] Zeeb G, Mitsch J, Wilhelm M, Kärger L, Henning F. Influence of gripper positions on the formation of wrinkles during the thermoforming process of thermoplastic UD-tape laminates. In: Materials research proceedings. vol. 54, Materials Research Forum LLC; 2025, p. 544–53. http://dx.doi.org/10.21741/9781644903599-59.

[9] Joppich T, Dörr D, van der Meulen L, Link T, Hangs B, Henning F. Layup and process dependent wrinkling behavior of PPS/CF UD tape-laminates during non-isothermal press forming into a complex component. In: AIP conference proceedings 1769, 170011. 2016, 170012. http://dx.doi.org/10.1063/1.4963568.

[10] Brands D, di Genova LG, Pierik ER, Grouve WJB, Wijskamp S, Akkerman R. Formability experiments for unidirectional thermoplastic composites. Key Eng Mater 2022;926:1358–71. http://dx.doi.org/10.4028/p-x3g086.

[11] Bussetta P, Correia N. Numerical forming of continuous fibre reinforced composite material: A review. Compos Part A: Appl Sci Manuf 2018;113:12–31. http://dx.doi.org/10.1016/j.compositesa.2018.07.010.

[12] Brooks RA, Wang H, Ding Z, Xu J, Song Q, Liu H, Dear JP, Li N. A review on stamp forming of continuous fibre-reinforced thermoplastics. Int J Lightweight Mater Manuf 2022;5(3):411–30. http://dx.doi.org/10.1016/j.ijlmm.2022.05.001.

[13] Boisse P, Akkerman R, Carlone P, Kärger L, Lomov SV, Sherwood JA. Advances in composite forming through 25 years of ESAFORM. Int J Mater Form 2022;15(3):99. http://dx.doi.org/10.1007/s12289-022-01682-8.

[14] Gunjal H, Singh G. Chapter 8 Review of optimization and simulation approaches for thermoplastic composite design. In: Green composites manufacturing. De Gruyter; 2024, p. 173–98.

[15] Guzman Maldonado E, Bigot N, Denis Y, Hamila N. 13 - Thermomechanical modeling and experimental characterization of continuous fiber-reinforced thermoplastic composites at forming temperatures. In: Wang P, Hamila N, editors. Advanced structural textile composites forming. Woodhead publishing series in composites science and engineering, Woodhead Publishing; 2025, p. 355–88. http://dx.doi.org/10.1016/B978-0-443-21578-0.00015-9.

[16] Tam AS, Gutowski TG. Ply-slip during the forming of thermoplastic composite parts. J Compos Mater 1989;23(6):587–605. http://dx.doi.org/10.1177/002199838902300604.

[17] Tam AS, Gutowski TG. The kinematics for forming ideal aligned fibre composites into complex shapes. Compos Manuf 1990;1(4):219–28. http://dx.doi.org/10.1016/0956-7143(90)90044-W.

[18] Gutowski T, Dillon G, Chey S, Li H. Laminate wrinkling scaling laws for ideal composites. Compos Manuf 1995;6(3–4):123–34. http://dx.doi.org/10.1016/0956-7143(95)95003-H.

[19] Hallander P, Akermo M, Mattei C, Petersson M, Nyman T. An experimental study of mechanisms behind wrinkle development during forming of composite laminates. Compos Part A: Appl Sci Manuf 2013;50:54–64. http://dx.doi.org/10.1016/j.compositesa.2013.03.013.

[20] Allaoui S, Boisse P, Chatel S, Hamila N, Hivet G, Soulat D, Vidal-Salle E. Experimental and numerical analyses of textile reinforcement forming of a tetrahedral shape. Compos Part A: Appl Sci Manuf 2011;42(6):612–22. http://dx.doi.org/10.1016/j.compositesa.2011.02.001.

[21] Boisse P, Hamila N, Vidal-Sallé E, Dumont F. Simulation of wrinkling during textile composite reinforcement forming. Influence of tensile, in-plane shear and bending stiffnesses. Compos Sci Technol 2011;71(5):683–92. http://dx.doi.org/10.1016/j.compscitech.2011.01.011.

[22] Dörr D, Schirmaier FJ, Henning F, Kärger L. A viscoelastic approach for modeling bending behavior in finite element forming simulation of continuously fiber reinforced composites. Compos Part A: Appl Sci Manuf 2017;94:113–23. http://dx.doi.org/10.1016/j.compositesa.2016.11.027.

[23] Dörr D, Henning F, Kärger L. Nonlinear hyperviscoelastic modelling of intra-ply deformation behaviour in finite element forming simulation of continuously fibre-reinforced thermoplastics. Compos Part A: Appl Sci Manuf 2018. http://dx.doi.org/10.1016/j.compositesa.2018.03.037.

[24] Guzman-Maldonado E, Hamila N, Naouar N, Moulin G, Boisse P. Simulation of thermoplastic prepreg thermoforming based on a visco-hyperelastic model and a thermal homogenization. Mater Des 2016;93:431–42. http://dx.doi.org/10.1016/j.matdes.2015.12.166.

[25] Dörr D, Joppich T, Kugele D, Henning F, Kärger L. A coupled thermomechanical approach for finite element forming simulation of continuously fiber-reinforced semi-crystalline thermoplastics. Compos Part A: Appl Sci Manuf 2019;125. http://dx.doi.org/10.1016/j.compositesa.2019.105508.

[26] Bigot N, Guzman-Maldonado E, Boutaous M, Xin S, Hamila N. A coupled thermo-mechanical modelling strategy based on alternating direction implicit formulation for the simulation of multilayered CFRTP thermo-stamping process. Appl Compos Mater 2022;29(6):2321–41. http://dx.doi.org/10.1007/s10443-022-10064-x.

[27] Sachs U, Akkerman R, Fetfatsidis K, Vidal-Sallé E, Schumacher J, Ziegmann G, Allaoui S, Hivet G, Maron B, Vanclooster K, Lomov SV. Characterization of the dynamic friction of woven fabrics: Experimental methods and benchmark results. Compos Part A: Appl Sci Manuf 2014;67:289–98. http://dx.doi.org/10.1016/j.compositesa.2014.08.026.

[28] Pierik ER, Grouve WJB, Wijskamp S, Akkerman R. Prediction of the peak and steady-state ply–ply friction response for UD C/PAEK tapes. Compos Part A: Appl Sci Manuf 2022;163:107185. http://dx.doi.org/10.1016/j.compositesa.2022.107185.

[29] Dörr D, Faisst M, Joppich T, Poppe C, Henning F, Kärger L. Modelling approach for anisotropic inter-ply slippage in finite element forming simulation of thermoplastic UD-tapes. In: AIP Proceedings of the 21th International ESAFORM Conference on Material Forming. 2018, http://dx.doi.org/10.1063/1.5034806.

[30] Schäfer B, Mitsch J, Kärger L. 3D solid-shell element for macroscopic composite forming simulation enabling thickness prediction. Compos Part A: Appl Sci Manuf 2025;109162. http://dx.doi.org/10.1016/j.compositesa.2025.109162.

[31] Mitsch J, Schäfer B, Kärger L. Rate-dependent 3D forming simulation of thermoplastic composite materials using visco-hyperelastic material modeling and 3D hexahedral solid-shell elements. Compos Part A: Appl Sci Manuf 2026;200:109306. http://dx.doi.org/10.1016/j.compositesa.2025.109306.

[32] Hsiao S-W, Kikuchi N. Numerical analysis and optimal design of composite thermoforming process. Comput Methods Appl Mech Engrg 1999;177(1):1–34. http://dx.doi.org/10.1016/S0045-7825(98)00273-4.

[33] Kärger L, Galkin S, Zimmerling C, Dörr D, Linden J, Oeckerath A, Wolf K. Forming optimisation embedded in a CAE chain to assess and enhance the structural performance of composite components. Compos Struct 2018;192:143–52. http://dx.doi.org/10.1016/j.compstruct.2018.02.041.

[34] Pfrommer J, Zimmerling C, Liu J, Kärger L, Henning F, Beyerer J. Optimisation of manufacturing process parameters using deep neural networks as surrogate models. Procedia CIRP 2018;72:426–31. http://dx.doi.org/10.1016/j.procir.2018.03.046.

[35] Zimmerling C, Dörr D, Henning F, Kärger L. A machine learning assisted approach for textile formability assessment and design improvement of composite components. Compos Part A: Appl Sci Manuf 2019;124:105459. http://dx.doi.org/10.1016/j.compositesa.2019.05.027.

[36] Zimmerling C, Poppe C, Stein O, Kärger L. Optimisation of manufacturing process parameters for variable component geometries using reinforcement learning. Mater Des 2022;214:110423. http://dx.doi.org/10.1016/j.matdes.2022.110423.

[37] Tan LB, Nhat NDP. Prediction and optimization of process parameters for composite thermoforming using a machine learning approach. Polymers 2022;14(14):2838. http://dx.doi.org/10.3390/polym14142838.
[38] Würth T, Freymuth N, Mitsch J, Dahlinger P, Hoang T, Neumann G, Kärger L. Algebraic Hierarchical Graph Neural Networks for Forming Simulation of Thermoplastic Composite Materials. Key Engineering Materials 2026;1050:31–42. http://dx.doi.org/10.4028/p-kaH2TN.
[39] Würth T, Freymuth N, Neumann G, Kärger L. Diffusion-based hierarchical graph neural networks for simulating nonlinear solid mechanics. 2025, http://dx.doi.org/10.48550/arXiv.2506.06045, arXiv:2506.06045.
[40] Sacks J, Welch WJ, Mitchell TJ, Wynn HP. Design and analysis of computer experiments. Statist Sci 1989;4(4):409–23. http://dx.doi.org/10.1214/ss/1177012413.
[41] Jones DR, Schonlau M, Welch WJ. Efficient global optimization of expensive black-box functions. J Global Optim 1998;13(4):455–92. http://dx.doi.org/10.1023/A:1008306431147.
[42] Forrester AIJ, Sóbester A, Keane AJ. Engineering design via surrogate modelling: A practical guide. 1st ed.. Wiley; 2008, http://dx.doi.org/10.1002/9780470770801.
[43] Forrester AIJ, Keane AJ. Recent advances in surrogate-based optimization. Prog Aerosp Sci 2009;45(1):50–79. http://dx.doi.org/10.1016/j.paerosci.2008.11.001.
[44] Shahriari B, Swersky K, Wang Z, Adams RP, de Freitas N. Taking the human out of the loop: A review of Bayesian optimization. Proc IEEE 2016;104(1):148–75. http://dx.doi.org/10.1109/JPROC.2015.2494218.
[45] Eriksson D, Pearce M, Gardner J, Turner RD, Poloczek M. Scalable global optimization via local Bayesian optimization. Adv Neural Inf Process Syst 2019;32. http://dx.doi.org/10.48550/ARXIV.1910.01739.
[46] Ament S, Daulton S, Eriksson D, Balandat M, Bakshy E. Unexpected improvements to expected improvement for bayesian optimization. Adv Neural Inf Process Syst 2023;36:20577–612. http://dx.doi.org/10.48550/ARXIV.2310.20708.
[47] Jagpal R, Evangelou E, Butler R, Loukaides EG. Preforming of non-crimp fabrics with distributed magnetic clamping and Bayesian optimisation. J Compos Mater 2022;002199832211036. http://dx.doi.org/10.1177/00219983221103637.
[48] Chen S, Thompson AJ, Dodwell TJ, Hallett SR, Belnoue JPH. Fast optimisation of the formability of dry fabric preforms: A Bayesian approach. Mater Des 2023;230:111986. http://dx.doi.org/10.1016/j.matdes.2023.111986.
[49] Chen S, Thompson AJ, Dodwell TJ, Hallett SR, Belnoue JPH. But how can I optimise my high-dimensional problem with only very little data? – A composite manufacturing application. Int J Solids Struct 2024;300:112941. http://dx.doi.org/10.1016/j.ijsolstr.2024.112941.
[50] Sobol' IM. On the distribution of points in a cube and the approximate evaluation of integrals. USSR Comput Math Math Phys 1967;7(4):86–112. http://dx.doi.org/10.1016/0041-5553(67)90144-9.
[51] Bruns C, Micke-Camuz M, Bohne F, Raatz A. Process design and modelling methods for automated handling and draping strategies for composite components. CIRP Ann 2018;67(1):1–4. http://dx.doi.org/10.1016/j.cirp.2018.04.014.
[52] Joppich TD. Beitrag zum Umformverhalten von PA6/CF Gelegelaminaten im nicht-isothermen Stempelumformprozess [Dissertation], Karlsruhe, Germany: Karlsruhe; 2019, http://dx.doi.org/10.5445/IR/1000097015.
[53] Dong C-s, Wang G-z. Curvatures estimation on triangular mesh. J Zhejiang Univ-Sci A 2005;6(S1):128–36. http://dx.doi.org/10.1631/jzus.2005.AS0128.
[54] Haanappel S. Forming of UD fibre reinforced thermoplastics: A critical evaluation of intra-ply shear [Dissertation], University of Twente; 2013, http://dx.doi.org/10.3990/1.9789036535014.
[55] Poppe C, Joppich T, Dörr D, Kärger L, Henning F. Modeling and validation of gripper induced membrane forces in finite element forming simulation of continuously reinforced composites. In: AIP conference proceedings. AIP conference proceedings, vol. 1896, 2017, 030002. http://dx.doi.org/10.1063/1.5007989.
[56] Mitsch J, Würth T, Wank JP, Kärger L. Validation of Thermoforming Simulation Models Prior to Parameterization Using Covariance-Based Input-Output Statistics – Assessing the Role of Thermomechanical Material Modeling. Materials Science Forum 2026;1182:1–11. http://dx.doi.org/10.4028/p-aI6KaL.
[57] Rasmussen CE. Gaussian processes in machine learning. In: Summer school on machine learning. Springer; 2003, p. 63–71. http://dx.doi.org/10.1007/978-3-540-28650-9_4.
[58] Hvarfner C, Hellsten EO, Nardi L. Vanilla Bayesian optimization performs great in high dimensions. 2024, http://dx.doi.org/10.48550/ARXIV.2402.02229, arXiv preprint arXiv:2402.02229.
[59] Frazier PI. A tutorial on Bayesian optimization. 2018, http://dx.doi.org/10.48550/ARXIV.1807.02811, arXiv preprint arXiv:1807.02811.
[60] Namura N, Takemori S. Regional expected improvement for efficient trust region selection in high-dimensional bayesian optimization. In: Proceedings of the AAAI conference on artificial intelligence. vol. 39, 2025, p. 19624–32. http://dx.doi.org/10.1609/aaai.v39i18.34161.